Performance Evaluation of Passive Tag to Tag Communications

Tarik Lassouaoui, Florin Hutu, Yvan Duroc, Guillaume Villemaud

IEEE Access
Multidisciplinary | Rapid Review | Open Access Journal

Received January 10, 2022, accepted January 29, 2022, date of publication February 7, 2022, date of current version February 22, 2022.

Digital Object Identifier 10.1109/ACCESS.2022.3149626

Performance Evaluation of Passive Tag to Tag Communications

TARIK LASSOUAOUI[1], (Student Member, IEEE), FLORIN DORU HUTU[1], (Senior Member, IEEE), YVAN DUROC[2], (Senior Member, IEEE), AND GUILLAUME VILLEMAUD[1], (Senior Member, IEEE)

[1]CITI, INSA Lyon, Inria, University of Lyon, 69621 Villeurbanne, France
[2]CNRS, Ampère, UMR5505, INSA Lyon, Ecole Centrale de Lyon, Université Claude Bernard Lyon 1, University of Lyon, 69622 Villeurbanne, France

Corresponding author: Tarik Lassouaoui (tarik.lassaouaoui@insa-lyon.fr)

This work was supported by the SPIE ICS-INSA Lyon IoT Chair.

ABSTRACT In the context of the UHF (Ultra High Frequency) passive RFID (Radio Frequency Identification) technology, recent works have proposed a new paradigm demonstrating the possibility to perform short distance tag to tag (T2T) communications. This paper presents a study that focuses on the performance evaluation of T2T systems. Without loss of generality as to the methodology followed, dipole antennas are considered here (assumed ideal in the theoretical part, then printed for the rest of the study). The results obtained show that the modulation depth, which can be considered as an evaluation metric for the T2T systems, is strongly impacted by three main parameters: the switching impedances (here chosen as short-circuit and open-circuit); the geometrical configuration constituted by the two tag antennas forming the T2T system; and also, the position of the external source on which the backscatter communication relies. As the modulation depth is very sensitive to these three parameters, which are more or less directly related, it is very difficult to predict the communication quality for a given configuration. For example, when the two tags are in parallel and the source is symmetrically positioned, the modulation depth shows a decreasing trend by oscillating when the distance between the tags increases from 0.1 λ to 1 λ (λ being the wavelength): with values going from 70% to less than 5%. As a consequence, from a very complete set of scenarios considered, the presented study helps to illustrate and explain the interactions of these parameters and their impact on the modulation depth. And at the same time, the paper provides guidelines for defining the specifications of such a system based on quantified results. The set is completed by introducing the BER (Bit Error Rate) as an evaluation metric by considering then a more complete T2T system (for instance listener tag including a non-coherent envelope detector).

INDEX TERMS Backscattering, passive tags, tag to tag communications, UHF RFID.

I. INTRODUCTION

The backscatter technique was first introduced by Stockman in 1948 [1] and quickly became the key technology for low-power wireless communication systems with a broad range of scenarios such as tracking devices, remote switches, low cost wireless sensor networks and, more generally, the Internet of Things (IoT) [2]–[4]. The main idea is to exploit the waves provided by a distant RF source (that can be dedicated or ambient) for backscattering, for instance reflecting more or less the RF signal, and so, to transmit the information by load modulation.

Ambient backscatter [5] has been emerging as a promising technology for low-energy communication systems. In this particular communication scenario, the backscatter transmitter sends the data by the means of an incoming electromagnetic (EM) field broadcasted by ambient RF sources, e.g. TV (television) or FM (Frequency Modulation) radio towers [5], Wi-Fi and even Bluetooth Low Energy [6], thereby reducing the system's power consumption.

Generally, the RF signals which are modulated by the backscatter transmitter usually have low levels [7]. Consequently, from the communication system point of view, the

The associate editor coordinating the review of this manuscript and approving it for publication was Renato Ferrero.

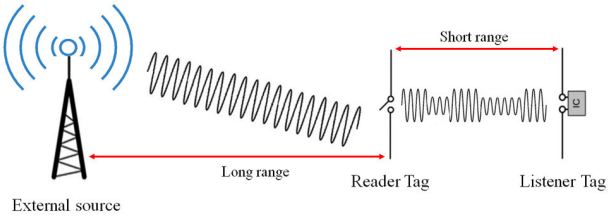

FIGURE 1. General principle of tag to tag communication.

effective signal to noise ratio is low and the data rate is limited. Several works have been carried out in order to overcome the ambient backscatter communication systems' limitations. For example, in [8], the authors designed a multi-antenna backscatter transmitter able to improve the communication performance and the transmission range by using multiple antennas. Their system is able to eliminate interference from the ambient RF signals thereby increasing the communication range of about 75%.

The RFID (Radio Frequency IDentification) technology is certainly the most emblematic example of backscatter communication systems [9]. Standardized technology, the RFID has become ubiquitous and widely deployed for applications as logistics, access control, real-time localization, sensor networks [10]. Nowadays, the sensitivity of the RFID tags' chips, for instance the minimum power that allows their activation, defines to a large extent the reading range. Recently, the sensitivity has been improved and reaches values below -22 dBm for the best current UHF RFID chips on the market [11].

For the first time, [12] demonstrated experimentally that two passive or semi-passive tags placed at a short distance between them can exchange data directly to each other in the absence of an RFID reader (Fig. 1). The concept is to achieve a communication between a reader tag (RT) and one or more listener tags (LTs) which are present in the RT's vicinity. The communication is established by backscattering an RF wave provided by a remote source and, based on commercial RFID tags, a reliable communication distance of about 25 mm (for instance 0.076 λ at 915 MHz, with λ is the wavelength) was established. However, the tag to tag (T2T) application scenarios demands to increase the communication range and also reliability. Consequently, a better understanding of the wireless propagation principles and of the coupling between the tag's antennas are necessary.

The T2T communication performance is dependent on the tag's relative position. Moreover, the tag's close vicinity creates an important EM coupling between their respective antennas. Consequently, the antenna characteristics such as the radiation pattern or the input impedance are modified. These modifications have an impact on the T2T's communication performance since the difference between the modulation states and implicitly the modulation depth is impacted [13].

A handful of works have been conducted in order to improve the communication range between the UHF RFID tags. In [14], a novel multi-phase backscattering technique is proposed to suppress phase cancellation and demonstrated the capability of T2T link to operate at longer distances (above three meters) in the presence of an excitation signal strength of only -20 dBm. In [15], the design of a power efficient demodulator is investigated to increase the T2T communication range with a modulation depth higher than 75%. In [16], a theoretical evaluation framework has been proposed as a tool allowing the performance evaluation of T2T radio links in terms of Bit Error Rate (BER). This study was extended by [17] which introduces analytical expressions for the error probability in the case of 2-ASK (Amplitude Shift Keying) modulation and considering that the LT consists of a coherent or non-coherent receiver demodulator.

In this paper, the impact of the relative position between two identical tags, which form the T2T system, as well as the impact of the position of the external source, which enables the communication between the tags by backscattering, are studied in depth. The objective is to evaluate the performance of T2T communication as a function of these two parameters by considering several possible scenarios.

The rest of the paper is organized as follows. Section II focuses on the LT's input impedance and highlights the impact of the mutual coupling between the tags. On the one hand, the relative position between the LT and the RT (for instance their separation distance, their orientation with respect to each other, their alignment), and on the other hand, the impedance load of the RT (considered here as short-circuited and open-circuited) are examined. The presented study is divided into two parts: the first one considers an ideal case (infinitely thin dipoles) and presents results based on theory and simplified simulations; the second one considers a practical case (printed dipoles) and presents results based on simulations and measurements. Section III evaluates the T2T system using the modulation depth as a metric. The impact on the modulation depth of three types of RT arrangement (for instance parallel, tilted, and staggered with respect to the LT) and the position of the external source are studied in detail from simulations. The influence of the LT's input impedance and the voltage gain on the modulation depth are particularly discussed and analysed in order to well-understand the observed variability on the modulation depth. In addition, the performance evaluation is extended by considering a system view of the T2T communications and the classical metric in digital communications, namely the BER. Finally, Section IV draws the conclusion and perspectives.

II. IMPACT OF THE MUTUAL COUPLING ON THE INPUT IMPEDANCE OF THE LISTENER TAG

In the T2T communications, the system formed by the two tags can be represented as an array of two coupled antennas. RT sends its information by switching its antenna's load on two different impedances. The choice of these two impedances will have an important impact on the T2T system performance. In this study, we consider them as a short-circuit (SC) and an open-circuit (OC), without loss of generality

as to the methodology followed and in agreement with the articles that have presented preliminary results on the subject treated. Depending on the load impedance (SC or OC) of the RT, the input impedance Z_{in} of the coupled antenna array, which corresponds to the impedance seen between the LT terminals, will be different. We will note $Z_{in,ON}$ when the RT load is an SC and $Z_{in,OFF}$ when the RT load is an OC; and in a more condensed form: $Z_{in,ON/OFF}$. In addition, Z_{in} will obviously also depend on the relative arrangement between the two antennas.

The following study in this section aims at investigating precisely this phenomenon, first in the case of ''ideal'' antennas (infinitely thin dipoles) in theory and simulation, and then in the case of printed dipole antennas in simulation and measurements. It should also be noted that the load impedance of the RT and the relative arrangement between the two antennas will also have an important impact on the voltage gain. Note that, the voltage gains are calculated from the far-field gains of the coupled antenna array (gain which will be denoted by G_{ON} and G_{OFF} respectively for a SC and an OC load; and in a more condensed form: $G_{ON/OFF}$); this will be detailed and clarified in section III.

A. THEORETICAL STUDY OF THE MUTUAL IMPEDANCE FOR INFINITELY THIN DIPOLES

In this section, the objective is to derive the analytical expression for the mutual impedance of the two identical coupled antennas regardless of their relative position. For this purpose, the two tag antennas are assumed to be ideal dipole antennas (called infinitely thin dipoles) and for their study the IEMF method is then applied as in [18] and [19], with the induced currents assumed to be sinusoidal.

As shown in Figure 2, the two antennas are placed in close proximity to each other, and more precisely are located at (x_{RT}, y_{RT}) and (x_{LT}, y_{LT}) respectively. The RT tilt's angle with respect to y axis is θ_{RT}. The distance between the two tags is given and considered as fractions of the wavelength. Under these considerations, the mutual impedance can be calculated by using (1).

$$Z_{21} = \int_{-\frac{l}{2}}^{\frac{l}{2}} E_{21} \cdot \sin\left[\beta\left(\frac{l}{2} - |s|\right)\right] ds \tag{1}$$

where:

$$E_{21} = \frac{1}{s}\left(E_x s_x + E_y s_y\right) \tag{2}$$

with

$$E_x = \frac{-\jmath \cdot 30 \cdot I_1}{dx + s_x}\left[-e^{-\jmath\beta r_1} \cdot \cos\alpha_1 - e^{-\jmath\beta r_2} \cdot \cos\alpha_2 + 2\cos\left(\frac{\beta l}{2}\right) \cdot e^{-\jmath\beta r} \cdot \cos\alpha\right] \tag{3}$$

and

$$E_y = \jmath \cdot 30 \cdot I_1\left[2\frac{e^{-\jmath\beta r}}{r} \cdot \cos\left(\frac{\beta l}{2}\right) - \frac{e^{-\jmath\beta r_1}}{r_1} - \frac{e^{-\jmath\beta r_2}}{r_2}\right] \tag{4}$$

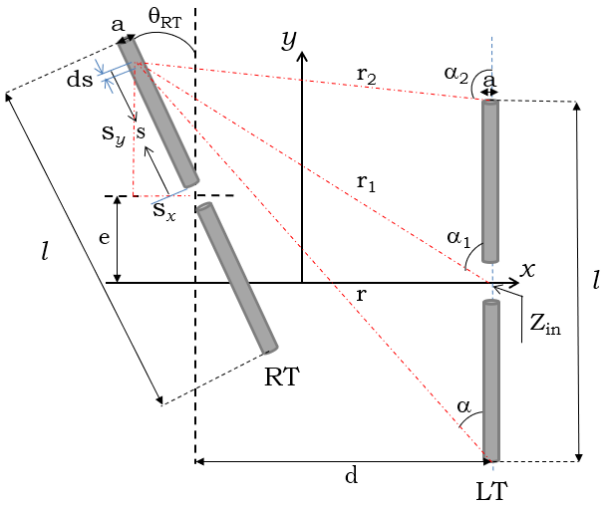

FIGURE 2. Geometrical configuration of two thin dipoles of the same length, RT's antenna is spaced and tilted with respect to LT's one.

where E_{21} is the electric field intensity present at each point s along RT's dipole due to the current along LT. l is length of the dipoles, β is the wave number. The distances r, r_1 and r_2 are deduced from the y axes to s. α, α_1 and α_2 are positive angles. s_x and s_y are the Cartesian's components of s. The following equations give the geometrical parameters corresponding to Fig. 2 to be inserted in equations from (1) to (4):

$$s_x = s \cdot \sin\theta_{RT} \tag{5}$$

$$s_y = s \cdot \cos\theta_{RT} \tag{6}$$

$$dx = x_{RT} - x_{LT} \tag{7}$$

$$r^2 = (dx + s_x)^2 + \left(y_{RT} + s_y\right)^2 \tag{8}$$

$${r_1}^2 = (dx + s_x)^2 + \left(y_{RT} + s_y + \frac{l}{2}\right)^2 \tag{9}$$

$${r_2}^2 = (dx + s_x)^2 + \left(y_{RT} + s_y - \frac{l}{2}\right)^2 \tag{10}$$

Finally, the mutual impedance Z_{21} is calculated by integrating the induced field E_{21} with respect to an incremental distance s along the RT's dipole.

Fig. 3 presents the variation of the mutual impedance Z_{21} as function of the separation distance d between the two parallel thin dipoles when the RT is short-circuited. The coupling effect in terms of mutual impedance is greatest for short distances and decreases progressively in ripples as the distance increases. In particular, zero values for the real part of the mutual impedance ($R_{21} = 0\ \Omega$) are observed for distances equal to 0.43 λ, 0.96 λ, 1.48 λ and 1.98 λ. It should be noted that when the RT is open-circuited, there is no impact of the mutual impedance. Fig. 4 shows the evolution of the mutual impedance as a function of the RT's antenna tilt θ_{RT} and for different spacing distances: $\frac{\lambda}{3}$, $\frac{2\lambda}{3}$ and λ. As expected, the spacing between the tags and their tilt changes significantly the mutual impedance Z_{21}. This impedance decreases while the distance d between the two antennas increases. This is due to the diminution of the EM coupling between the antennas

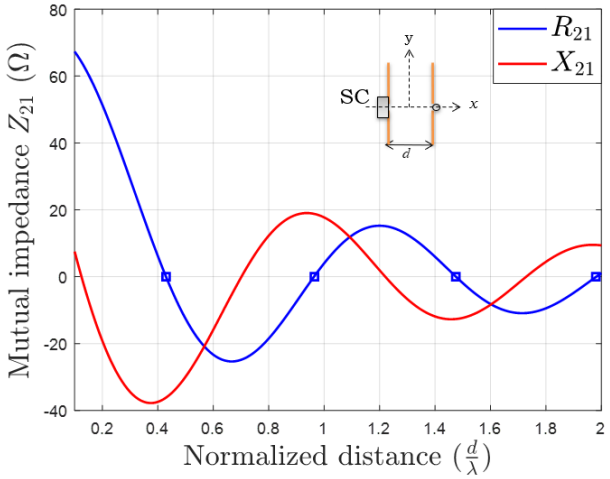

FIGURE 3. Real part (R_{21}) and imaginary parts (X_{21}) of the mutual impedance Z_{21} as function of separation distance d (normalized value) between the dipoles when the reader tag is short-circuited.

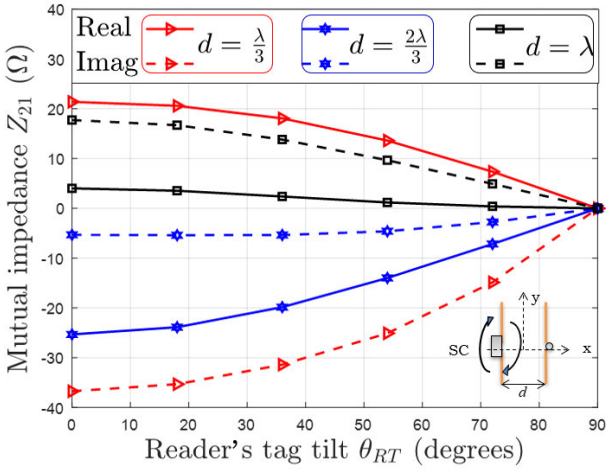

FIGURE 4. Real part (R_{21}) and imaginary parts (X_{21}) of the mutual impedance Z_{21} as function of θ_{RT} tilt angle of the RT's dipole for several separation distances d (normalized value) between the dipoles when the reader tag is short-circuited.

and this will impact the effective EM characteristics of the system (antennas parameters such as the radiation pattern and matching properties).

It should be also noted that there are two ways to express the tilt angle of the RT's antenna. For example, $\theta_{RT} = 45°$ is the same physical configuration as $\theta_{RT} = 225°$. However, the value of Z_{21} is of opposite sign. This is due to the voltage reference [18]. In order to avoid confusion, θ_{RT} is defined such that it is not exceeding 90^o.

Finally, the knowledge of the mutual impedance Z_{21} according to the relative position of the tags allows to easily deduce the LT's input impedance as detailed in the following section.

B. CASE OF ELECTRICALLY THIN DIPOLES: THEORY AND SIMULATIONS

From the above study, the input impedance Z_{in} is calculated for different configurations. The theoretical results obtained

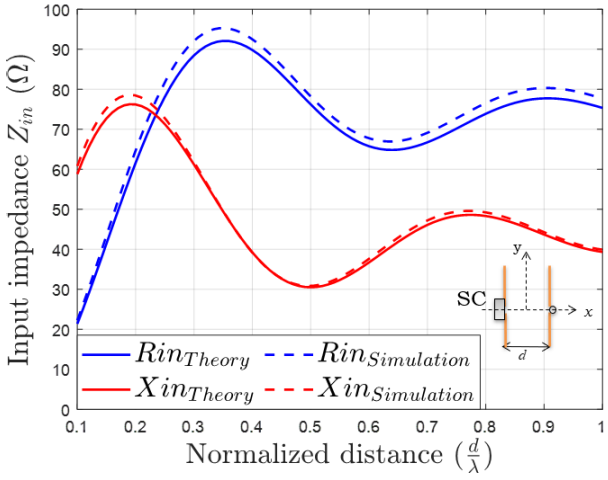

FIGURE 5. Calculated and simulated input impedance Z_{in} of the listener tag. The resistance (R_{in}) and reactance (X_{in}) are plotted as function of separation distance d (normalized value) between the two infinitely thin dipoles when the reader tag is short-circuited.

are compared with the results of EM simulations, performed for this part with the free software 4NEC2 (which is based on the method of moments, MoM).

To be more precise, the two nearly coupled tags can be seen as a matrix of two antennas which are considered identical. Assuming the reciprocity between the two tag's identical antennas, the self (Z_{11}, Z_{22}) and the mutual (Z_{12}, Z_{21}) impedances of both antennas are equal. Considering the two RT's antenna loads ($Z_{L,ON}$ for the SC and $Z_{L,OFF}$ for the OC), the LT's input impedance Z_{in} can be written as follows:

$$Z_{in,ON/OFF} = Z_{11} - \frac{Z_{21}Z_{12}}{Z_{22} + Z_{L_{ON/OFF}}} \tag{11}$$

The real and imaginary parts of the LT's input impedance as function of the separation distance d between the two dipoles are shown in Fig. 5 and Fig. 6, when the RT is in SC and OC mode respectively. As expected, thanks to the study of the mutual impedance, the presence of the RT in SC mode affects significantly the LT's input impedance at short distances; and this effect decays when the separation distance between the tag's antennas increases. The RT in OC mode has no impact on the LT's input impedance; indeed, no sinusoidal current is generated.

Thus, as a first approximation, these two methods (for instance theoretical calculation and simulation with 4NEC2 software) allow to quickly evaluate the impact of the tags' arrangements on the LT's input impedance. However, they are limited and cannot consider arbitrary complex antennas. For further study and also for practical considerations, simple but realistic antennas will now be considered. Consequently, the theoretical part will not be developed, the simulation steps will be performed with a more accurate EM simulator, CST Microwave Studio (based on the finite element method, FEM), and will be compared with measurement results beforehand.

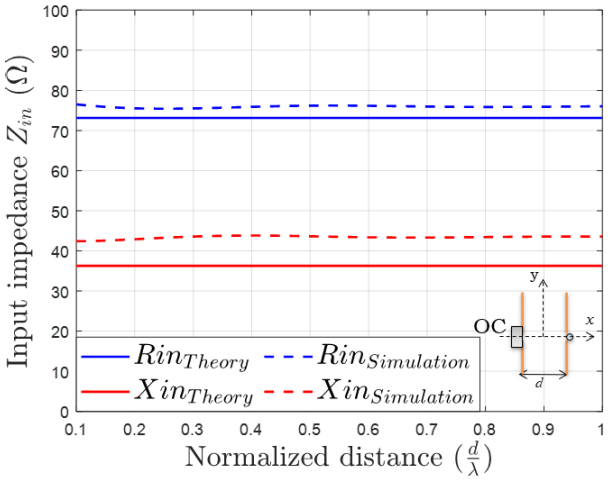

FIGURE 6. Calculated and simulated input impedance Z_{in} of the listener tag. The resistance (R_{in}) and reactance (X_{in}) are plotted as function of separation distance d (normalized value) between the two infinitely thin dipoles when the reader tag is open-circuited.

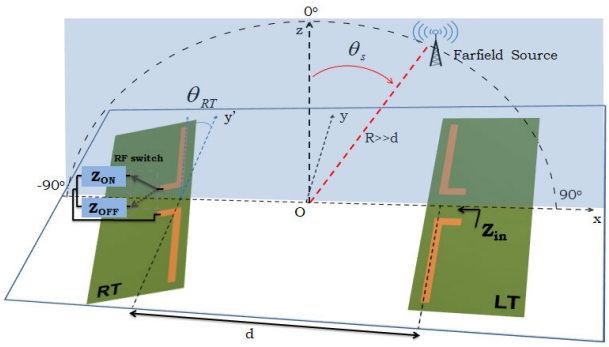

FIGURE 7. Geometrical configuration of two printed dipoles. The RT's antenna takes different arrangements (parallel, tilted and staggered) with respect to LT's one. The external source orientation is considered relative to the z.

C. CASE OF PRINTED DIPOLES: EM SIMULATIONS AND MEASURES

Since commercial RFID tag antennas are often based on dipole antennas (incorporating some improvements: e.g. miniaturization techniques with the use of folded dipoles or matching techniques with an additional loop in the antenna design), for the remainder of the study including an experimental part, simple antenna dipoles, for instance printed dipoles, are considered. It is important to note that, depending on the tag's antenna configuration considered in practice, the observed characteristics will probably be different compared to those presented here, but both the methodology and the trend of the observed behaviour remain valid.

The considered antennas of the tags are printed dipoles on FR4 material with substrate dimensions 150 mm × 10 mm and copper printed circuit tracks 134 mm × 1 mm). Fig. 8 shows the simulation models and the photos of the two closely coupled antennas in each modulation states (SC and OC) of RT. As shown by Fig. 9, each printed dipole was designed such that its self-impedance Z_{11} is 50 Ω at the frequency of 868 MHz. Fig. 10 shows the reflection coefficient S11

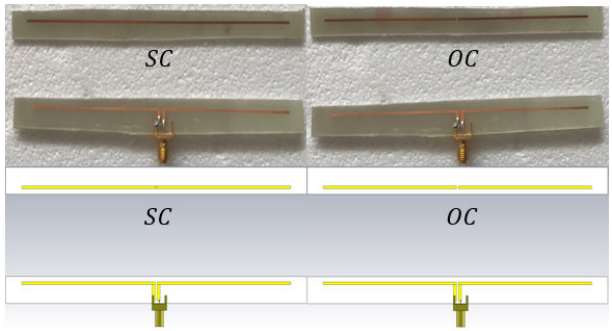

FIGURE 8. Simulation models and the photos of the two closely coupled antennas in each modulation states (SC and OC) of RT.

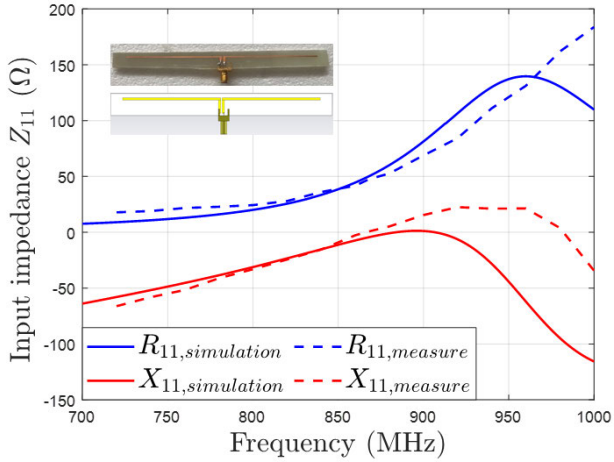

FIGURE 9. Simulated and measured self impedance Z_{11} of the printed dipole. The resistance (R_{11}) and reactance (X_{11}) are plotted as function of the frequency.

and a relatively good agreement between simulation and measurement results.

Finally, using this antenna for the two tags, the T2T system is built up and the LT's input impedance is simulated and measured for the two cases considered (RT in SC mode and in OC mode). Assuming a parallel arrangement, Fig. 11 and Fig. 12 show the real and imaginary parts of the input impedance Z_{11} as a function of the distance d between the antennas and with respect to the two RT's loads. The simulation results are consolidated with the experimental ones and we can observe a good agreement between the two. Moreover, it should be noted that the observed behavior is very similar to that obtained in the previous more idealistic case. In particular, the weak impact of the presence of the RT in short-circuit and on the contrary its more important impact when it is in short-circuit.

III. PERFORMANCE EVALUATION OF THE T2T COMMUNICATION SYSTEM

Based on the previous study, this section aims at evaluating the performance of T2T communication by considering a given scenario, for instance the geometrical configuration constituted by the two tag antennas forming the T2T system, and also, the position of the external source on which the

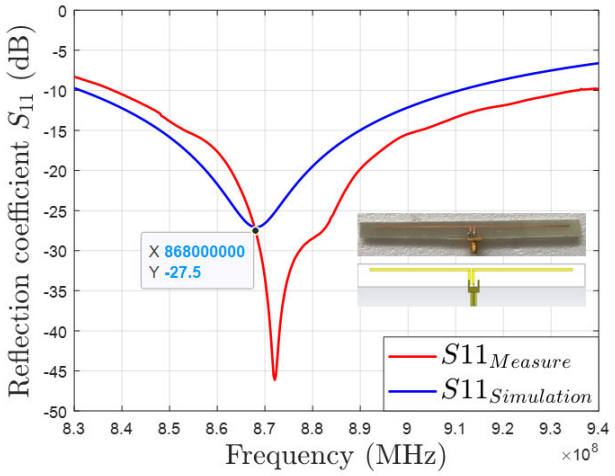

FIGURE 10. The simulated and measured reflection coefficient S_{11} of the tag's printed dipole.

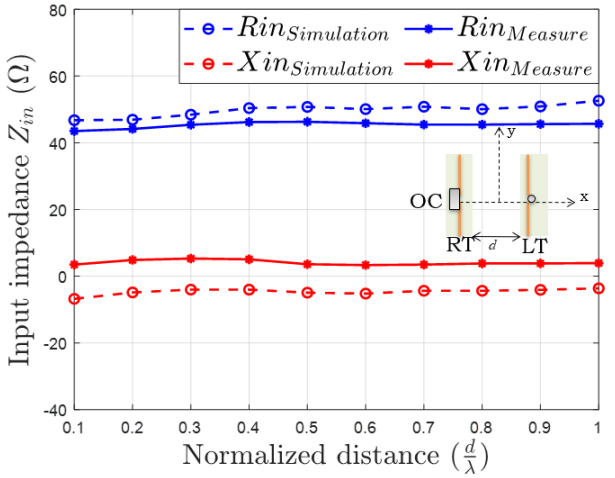

FIGURE 11. Simulated and measured input impedance Z_{in} of the listener tag. The resistance (R_{in}) and reactance (X_{in}) are plotted as function of separation distance d (normalized value) between the two printed dipoles when the reader tag is open-circuited.

backscatter communication relies. Taking up the diagram presented in Fig. 2, Fig. 7 gives an updated illustrated representation with the printed dipoles and the external RF source which emits the continuous wave, clarifying and completing the important parameters considered for the different configurations envisaged (including d the distance between the two tags, θ_{RT} the title angle of RT, and θ_s the angle defining the source position relative to the z axis in the xOz plane).

It is worth noting that, so far, we have considered for the illustrations the case where the tags are aligned. Using the same method, further illustrations of the variation of LT's input impedance can be found in [20] for cases where the tags are not aligned but tilted and staggered, considering RT in SC mode and OC mode. In this section, the presented results will be more complete and will illustrate the different configurations considered. Note also that throughout the section, we have been mindful of practicalities and have been careful not to present unrealistic scenarios that would involve the

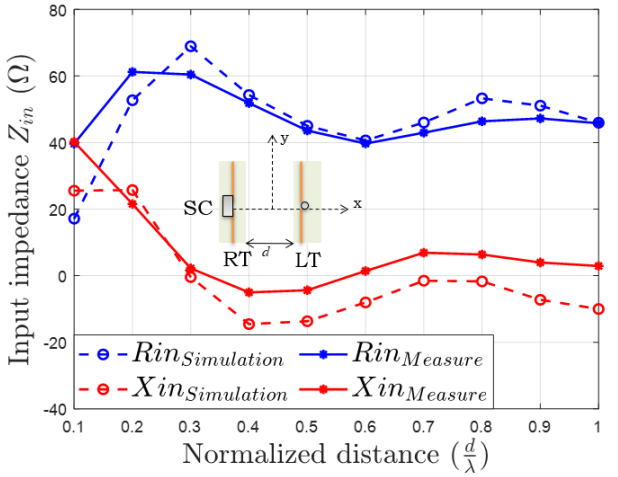

FIGURE 12. Simulated and measured input impedance Z_{in} of the listener tag. The resistance (R_{in}) and reactance (X_{in}) are plotted as function of separation distance d (normalized value) between the two printed dipoles when the reader tag is short-circuited.

tags overlay (for example, in Fig. 13, when we assumed an θ_{RT} angle of 20° we made sure that at the smallest distance considered, there was no contact between the tags).

A. MODULATION DEPTH AS METRIC OF COMMUNICATION PERFORMANCE

The modulation depth is used as an evaluation metric. This parameter plays a particularly crucial role in the communication performance of T2T systems which rely on 2-ASK modulations. Indeed, on the one hand, these systems are very sensitive to noise because the signals involved are of low to very low energy, and on the other hand, in order to keep the passive character of the tags, the demodulator is often a simple envelope detector. Thus, the greater the modulation depth (for instance the greater the separation of information levels), the more robust the communication will be to channel noise and the information will be easy to detect.

Recall that the principle of a T2T communication is as follows: as a result of the RT's commutation between the two loads, the input voltage at LT toggles between two levels, here noted A_{ON} and A_{OFF}, corresponding to a 2-ASK modulation. Besides the two levels A_{ON} and A_{OFF} are function of the LT's antenna input impedance $Z_{in,ON/OFF}$ and the two antennas voltage gain $G_{ON/OFF}$, as described in equation (12).

$$A_{ON/OFF} = A_{in} \cdot G_{ON/OFF} \left| 1 - \left(\frac{Z_{in,ON/OFF} - Z_0}{Z_{in,ON/OFF} + Z_0} \right) \right| \quad (12)$$

where A_{in} is the input voltage at LT delivered by the external source and Z_0 the reference impedance which was considered 50 Ω, without loss of generality.

And finally, the modulation depth D is defined in terms of the two voltage levels A_{ON} and A_{OFF}, as follows:

$$D = \frac{|A_{ON} - A_{OFF}|}{Max(A_{ON}, A_{OFF})} \quad (13)$$

TABLE 1. Summary of T2T performance in terms of modulation depth for parallel arrangement between tags in function of the separation distance and comparison with literature results.

Reference	Substrate type	Frequency (MHz)	Source position θ_s	Separation distance ($\frac{d}{\lambda}$)									
				0.1	0.2	0.3	0.4	0.5	0.6	0.7	0.8	0.9	1
[12]	Rogers 4003C	915	Supposed at 90°	58%	42%	39%	25%	19%	15%	–	–	–	–
[13]	Unknown	870	Supposed at 90°	51%	47%	35%	22%	20%	19%	19%	18%	15%	11%
This article.	FR4	868	90°	34%	43%	33%	18%	13%	34%	3%	21%	16%	6%

It should be noted that, for the study presented, the ON and OFF states refer to the load impedances of the RT, for instance SC and OC respectively.

In order to study the influence of the two tags' relative position on the modulation depth D, different scenarios are simulated. Note that for all figures, the modulation depth will be expressed as a percentage and noted as Modulation depth (%).

First, the RF source is fixed, perpendicular to the plane containing the two tags ($\theta_s = 0°$). Fig. 13 presents the evolution of the modulation depth D as function of the distance d between the tags and three types of RT arrangement: RT is parallel to LT; RT is tilted by $\theta_{RT} = 20°$; RT is staggered by 0.2 λ. As a priori expected, the maximum modulation depth is obtained for short distances between the tags. It is noticeable that the higher modulation depth is obtained with the parallel arrangement. Globally, the modulation depth decreases similarly by the distance d and those for the considered three configurations (for instance parallel, tilt, stagger). It should be noted that the lowest values of the modulation depth ($D \leq 5\%$) are observed for the distance 0.4 λ and 0.9 λ. This result is coherent with the input impedance shown in the Fig. 12. Indeed, for these two distances where the mutual coupling is negligible, the input impedance Z_{in} is approximately equal to Z_{11} for the SC and OC modes. As a consequence, the two states are the same and the modulation depth is also zero. Fig. 14 shows the evolution of the modulation depth D for RT tilts (with respect to a vertical position) varying from $\theta_{RT} = 0°$ to 70°, and also, for three distances d (0.3 λ, $\frac{\lambda}{2}$, and λ) between the two tags.

For these three distances, the modulation depth D decreases significantly while the RT's tilt angle θ_{RT} increases. This first set of results (Fig. 13 and Fig. 14) demonstrates the sensitivity of the T2T communication system with respect to the tags arrangement. In addition, the parallel configuration is more favourable as it maximizes the modulation depth D.

The study is now completed by considering changes in the orientation of the illuminating source, a parameter that also has a strong influence on the modulation depth. From the Fig. 15 to Fig. 17, the three previous scenarios are considered: RT is parallel to LT (Fig. 15), RT is staggered by 0.2 λ (Fig. 16), and RT is tilted by $\theta_{RT} = 20°$ (Fig. 17). For each case, the modulation depth D is illustrated as the distance between the tags (for instance the normalized distance $\frac{d}{\lambda}$ which varies between 0.1 and 1 with a step of 0.1) considering six positions of the distant RF source (for instance $\theta_s = -60°$, $-30°$, 0°, 30°, 60°, 90°). Furthermore, each considered scenario, the best case (for instance D maximum for a given

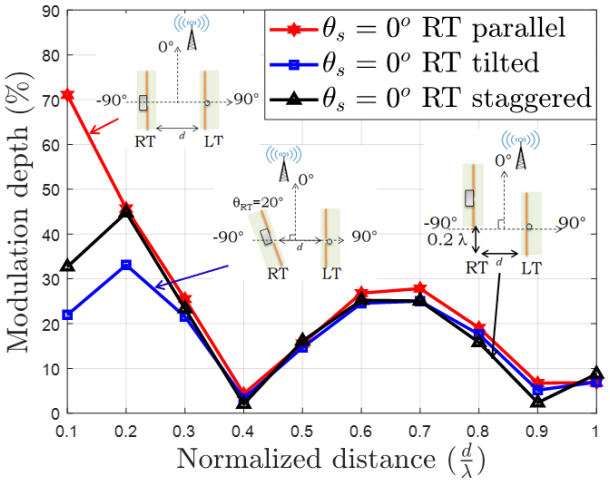

FIGURE 13. Simulation results of the modulation depth *D* as function of the normalized distance *d* between tags when RT is parallel to LT, RT is tilted by $\theta_{RT} = 20°$ and RT tag staggered by 0.2 λ.

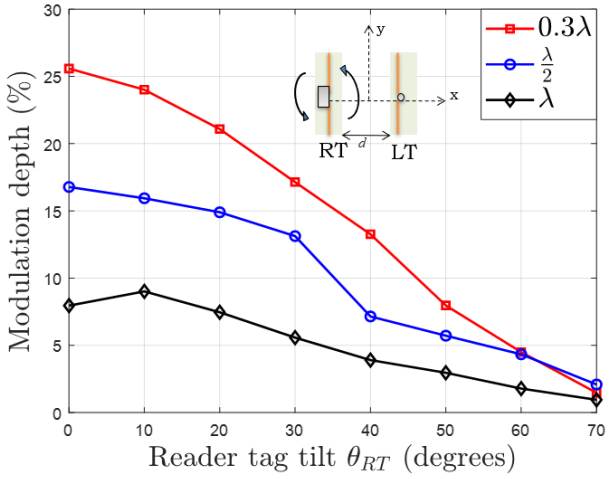

FIGURE 14. Simulation results of the modulation depth *D* as function of the RT antenna's tilt θ_{RT} with different distances *d* (normalized value) between tags (0.3 λ, $\frac{\lambda}{2}$ and λ).

distance) is highlighted: the corresponding angle is noted θ_{opt}. It is worth noting that this most advantageous case is not systematically when $\theta_s = 0°$. Indeed, for instance, and for the three RT's illustrated configurations, we can remark that for $d = 0.4$ λ (about 14 cm at 868 MHz) the modulation depth can be increased by changing the source orientation. For the separation distances above 0.2 λ, the optimal angle of the source θ_s is the same for the three RT's configurations. The minimum modulation depth D is 21% and is obtained for the maximal separation distance ($d = \lambda$). This set of

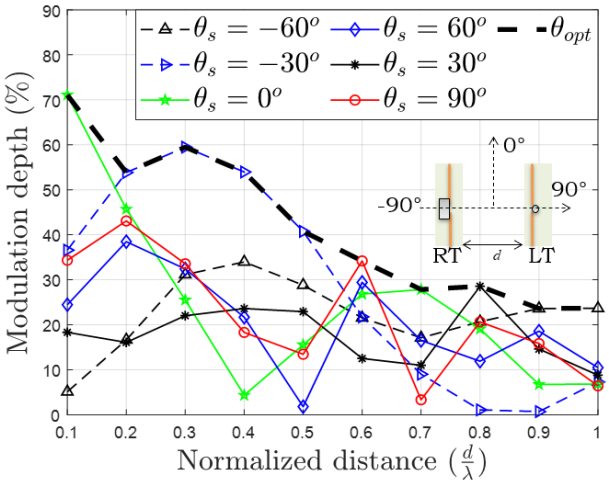

FIGURE 15. Simulation results of the modulation depth *D* as function of the normalized distance *d* between tags and the position of the distant RF source θ_s when RT is parallel to LT.

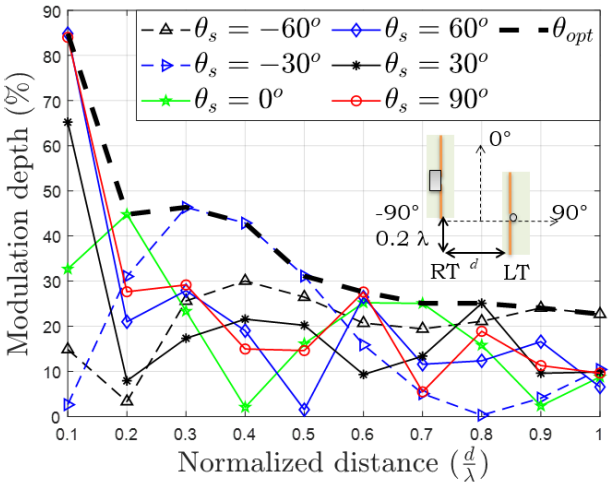

FIGURE 16. Simulation results of the modulation depth *D* as function of the normalized distance *d* between tags and the position of the distant RF source θ_s when RT is parallel to LT with a stagger of 0.2 λ.

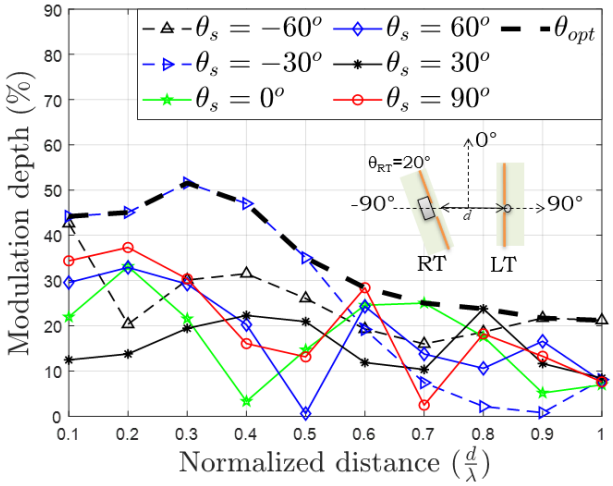

FIGURE 17. Simulation results of the modulation depth *D* as function of the normalized distance *d* between tags and the position of the distant RF source θ_s when RT is tilted by $\theta_{RT} = 20°$.

results also shows that a parallel arrangement between the tags will enable to maximize easily the modulation depth. Moreover, the T2T communication quality, regardless tags configuration (here, considering spacing, stagger and tilt cases), can be improved by tuning the source orientation θ_{opt} with respect to the tag's position. The results presented in Fig. 16 to Fig. 17 confirm the fact that the external source need to change its position in the tags' vertical plane in order to achieve θ_{opt}, and thus to maximize the modulation depth whatever the tags' relative position. Consequently, the chance that the two tags are communicating together is maximized.

In addition, all these results also show that the knowledge of the variation of the modulation depth with respect to the two tags configuration could be used, for instance, as a source of information. Indeed, the activation of T2T communication could be translated as a proper or tolerable alignment between the tags.

Finally, Table 1 highlights and compares with the literature [12], [13] the values of the modulation depth D as a function of separation distance d for the parallel tag arrangement when the source is oriented at $\theta_s = 90°$ (and assumed to be so oriented likewise for the two references cited which do not give explicitly this information, although critical as highlighted in this work). The results we present here are taken from Figure 15. Comparing the results achieved here with those of the literature, some differences are observed especially for the distances 0.1 λ, 0.6 λ, 0.7 λ and λ. It should be noted that the considered antennas, as well as the employed substrates, are not the same in the three studies. If the strict decrease of the modulation depth when the distance increases may seem ''natural'' because the coupling between the antennas also decreases, we will see later (Section III.B) that the analysis is not so simple and must be completed because, in particular, the impact of the gain is also to be considered.

B. ANALYSIS OF THE RESULTS AND DISCUSSION

As shown in the presented results, the modulation depth, which is a fundamental parameter impacting the T2T communication, is highly variable depending on the considered scenario (for instance the considered relative arrangement between the tags and the external source position). Indeed, the modulation depth is a function of both the LT's input impedance and the voltage gain of the coupled dipole; and consequently, its variations are complex and very difficult to predict.

In order to illustrate more precisely the observed variability of the modulation depth, let us imagine the following scenario: the tags are arranged in parallel and separated by a distance of 0.4 λ. The difference, ΔZ_{in}, between the values of the LT's input impedances when RT is open-circuited (Fig. 11) and when RT is short-circuited (Fig. 12) is nearly zero. This result is consistent because for this distance between tags, whatever the RT load, we observe that the mutual

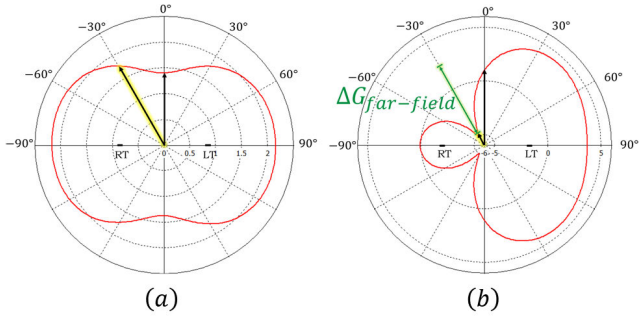

FIGURE 18. The radiation pattern of the coupled tags at $d = 0.4\ \lambda$ when the RT tag is loaded by: a) an open-circuit (OC) and b) a short-circuit (SC).

impedance is very low ($Z_{12} = Z_{21} \approx 0\ \Omega$); therefore: $Z_{in,ON} \approx Z_{in,OFF} \approx Z_{11}$ and $\Delta Z_{in} = Z_{in,ON}\text{-}Z_{in,OFF} \approx 0\ \Omega$.

Now, if we consider the modulation depth for this configuration in Fig. 15, we notice that it varies significantly between 4% (worst configuration with the source at $\theta_s = 0°$) and 54% (best configuration with the source at $\theta_s = -30°$). Let us then add in the analysis this effect of the position of the source. Note that the presence of the RT in short-circuit acts as a parasitic element and therefore impacts the overall radiation pattern, which is not the case when RT is in open-circuit. Fig. 18 shows the 2D radiation pattern (vertical plane) of the gain for the coupled tags (always considered as arranged in parallel with a distance of 0.4 λ) and considering the two RT loads: Fig. 18(a) with G_{OFF} for the OC mode and Fig. 18(b) with G_{ON} for the SC mode. For a given source direction, compare the difference in gains, $\Delta G = \mid G_{ON}\text{-}G_{OFF} \mid$. For instance, for $\theta_s = 0°$, $\Delta G = 0.34$ dB and for $\theta_s = -30°$, $\Delta G = 6.77$ dB. Therefore, in this case, since $\Delta Z_{in} \approx 0\ \Omega$ for this tags' arrangement, from (12) and (13) we can deduce that the gain difference ΔG is the determining factor of the modulation depth.

In conclusion, the LT's input impedance and the voltage gain jointly determine the modulation depth. Furthermore, as the distance between the tags increases (whether they are aligned or in some other configuration), the mutual coupling between the two tags decreases and, as a result, the modulation depth is increasingly determined by the source position and thus the gain of the T2T system.

C. BIT ERROR RATE AS METRIC OF OVERALL SYSTEM PERFORMANCE

In order to extend the proposed study and to consider a global T2T system, it is possible to exploit the obtained results in order to determine the BER which is a well-known metric in the field of digital communications [17]. This parameter depends on the modulation depth but also on the type of radio receiver used. The interest of this approach is to offer a way to couple the domains of electromagnetism, antennas, electric circuit, system; and, therefore, to have a methodology allowing to evaluate the global performance of a T2T system. The presented results assume that the demodulator of the LT is based on a passive non-coherent envelope receiver. Further

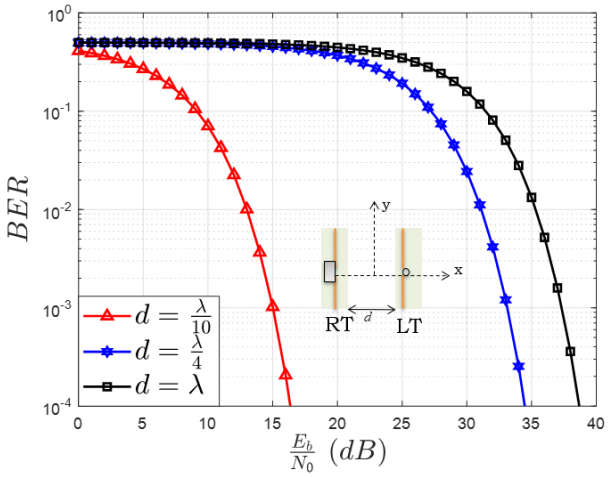

FIGURE 19. Bit error rate given as function of $\frac{E_b}{N_0}$ for different spacing d between tags ($\frac{\lambda}{10}$, $\frac{\lambda}{4}$ and λ) when the source orientation is $\theta_s = 0°$.

assuming that the collected information signal is degraded by an Additive White Gaussian Noise (AWGN), the BER can be determined as in [16] and can be rewritten as a function of the modulation depth as follows:

$$BER_{NC} = \frac{1}{2} \cdot \exp\left(-\frac{A_{in}A_{ON}T_s}{8N_0} \cdot \frac{D^4 - 2D^3 + 2D^2}{2 - D}\right) \quad (14)$$

with A_{in} the RF source's voltage, A_{ON} the voltage of the high level "1", T_s is the bit time, D the modulation depth and N_0 is the noise power. It can be directly deduced from this formula that the BER is a strictly decreasing function as the modulation depth increases.

For illustrating, the BER variation has been calculated theoretically by considering that the tags are illuminated by a CW having a power level such that the incident power at the RT's level is −50 dBm. The used values of the input impedance $Z_{in,ON/OFF}$ and of the gain $G_{ON/OFF}$ are taken from the simulation results obtained by the EM simulations. The Fig. 19 shows the BER evolution for three separation distances d ($\frac{\lambda}{10}$, $\frac{\lambda}{4}$ and λ) between the tags, and this, considering the RF source perpendicular to the plane containing the two tags ($\theta_s = 0°$). As expected, the best performance in terms of BER is obtained for the distance $\frac{\lambda}{10}$ between the tags for which the modulation depth is highest in the examples considered here (see Fig. 15), and inversely the worst case is obtained for the distance λ for which the modulation depth is the lowest. Furthermore, Fig. 20 shows the BER when the tags are spaced by a distance $\frac{\lambda}{4}$ and considering three source orientations ($\theta_s = 0°$, $-30°$ and $-60°$). As expected from Figure 15 and by a reasoning similar to the previous section (for instance, the higher ΔG is the greater the modulation depth, which leads to a lower BER if no major impact is observed on the signal-to-noise ratio), the orientation of the source $\theta_s = -30°$ leads to better performance. Specifically, the improvement observed here between a source located such that $\theta_s = -30°$ and a source at $\theta_s = 0°$, assuming for

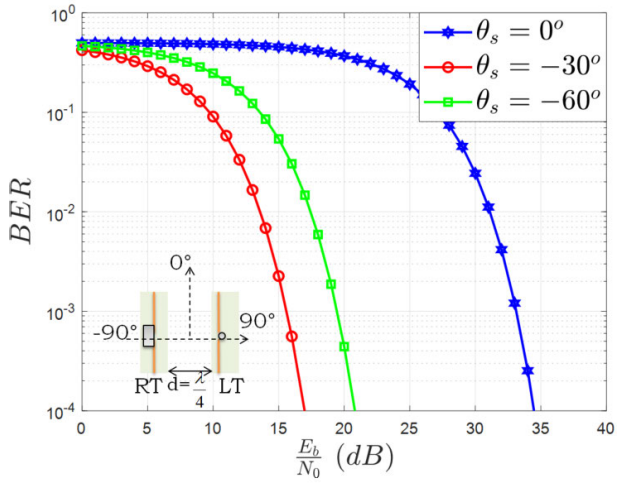

FIGURE 20. Bit error rate given as function of $\frac{E_b}{N_0}$ while tags are spaced by 0.4λ and for different source orientations θ_s (0°, −30° and −60°).

FIGURE 21. Example of a potential T2T system. The illustrated idea is to detect a potential misplacement (or even absence) of the safety equipment, and thus, the user is warned.

example that the objective is to achieve a BER equal to 10^{-3}, is equal to 17.5 dB.

IV. CONCLUSION

In the context of the new passive RFID T2T systems, this paper investigated the impact of the relative position between the tags (and thus their mutual coupling), and the orientation of the external RF source, on the communication performance. The modulation depth, which can be considered as an evaluation metric for the T2T systems, is strongly impacted by three main parameters: the switching impedances; the geometrical configuration constituted by the two tag antennas forming the T2T system; and also, the position of the external source. As the modulation depth is very sensitive to these three parameters, which are more or less directly related, it is very difficult to predict the communication quality for a given configuration.

For example, when the two tags are in parallel and the source is symmetrically positioned, the modulation depth shows a decreasing trend by oscillating when the distance between the tags increases from 0.1 λ to 1 λ (λ being the wavelength): with values going from 70% to less than 5%. But if the source position is modified, then the modulation depth varies significantly and it is possible to determine more optimal configurations than others. This example shows that T2T systems show unstable performance depending on the configurations considered, which is a limiting factor in practice. Future applications will necessarily have to take these aspects into account. It should also be noted that the ISO 18000-6C standard requires that RFID readers use a modulation depth greater than 80%. However, in [21], an optimized demodulator is proposed to operate with a modulation depth close to 20%. The deployment of T2T systems will certainly require such approaches and new advances for passive receivers.

As a consequence, from a very complete set of scenarios considered, the presented study helps to illustrate and explain the interactions of these parameters and their impact on the modulation depth. And at the same time, the paper provides guidelines for defining the specifications of such a system based on quantified results. The set is completed by introducing the BER as an evaluation metric by considering then a more complete T2T system including here as demodulator a non-coherent envelope detector.

In terms of perspectives, it could be interesting to consider not simple load impedances (for instance short-circuit and open-circuit) but complex (and more realistic in practice) impedances in order to study if it is possible to improve the modulation depth. On the other hand, but at the expense of complexity, the addition of a parasitic element near the antennas could also provide an extra degree of freedom to differentiate between the two modulation states. Note also that there are several potential applications of T2T communications, described for example in the perspective section of [12]. Others are to be imagined in order to find an application context that is meaningful for the deployment of T2T systems.

In this study, to give an example and to illustrate our point in clear manner, we propose as a potential application a powerless system allowing the monitoring of the use of security equipment (Fig. 21). Communication between the tags, which are attached to each piece of safety equipment, is only established if their relative position is in the correct configuration. By checking the communication between the tags, for example when the person passes through a gate on which the RF source is fixed (for instance with a known position), a potential misplacement or oversight by the user can be avoided. Such applications remain to be developed but the results presented here can provide both limitations and guidelines to follow.

REFERENCES

[1] H. Stockman, "Communication by means of reflected power," *Proc. IRE*, vol. 36, no. 10, pp. 1196–1204, Oct. 1948.
[2] K. V. S. Rao, "An overview of backscattered radio frequency identification system (RFID)," in *Proc. Asia Pacific Microw. Conf. (APMC)*, 1999, pp. 746–749.
[3] J. Niu and G. Y. Li, "An overview on backscatter communications," *J. Commun. Inf. Netw.*, vol. 4, no. 2, pp. 1–14, Jun. 2019.
[4] X. Lu, D. Niyato, H. Jiang, D. I. Kim, Y. Xiao, and Z. Han, "Ambient backscatter assisted wireless powered communications," *IEEE Wireless Commun.*, vol. 25, no. 2, pp. 170–177, Apr. 2018.

[5] V. Liu, A. Parks, V. Talla, S. Gollakota, D. Wetherall, and J. R. Smith, "Ambient backscatter: Wireless communication out of thin air," *Comput. Commun. Rev.*, vol. 43, pp. 39–50, Aug. 2013.
[6] J. F. Ensworth and M. S. Reynolds, "Every smart phone is a backscatter reader: Modulated backscatter compatibility with Bluetooth 4.0 low energy (BLE) devices," in *Proc. IEEE Int. Conf. RFID (RFID)*, Apr. 2015, pp. 78–85.
[7] D. T. Hoang, D. Niyato, P. Wang, D. I. Kim, and Z. Han, "Ambient backscatter: A new approach to improve network performance for RF-powered cognitive radio networks," *IEEE Trans. Commun.*, vol. 65, no. 9, pp. 3659–3674, Sep. 2017.
[8] N. Fasarakis-Hilliard, P. N. Alevizos, and A. Bletsas, "Coherent detection and channel coding for bistatic scatter radio sensor networking," *IEEE Trans. Commun.*, vol. 63, no. 5, pp. 1798–1810, May 2015.
[9] K. Finkenzeller, *RFID Handbook: Fundamentals and Applications in Contactless Smart Cards and Identification*. New York, NY, USA: Wiley, 2003, p. 427.
[10] L. Yan, Y. Zhang, L. T. Yang, and H. Ning, *The Internet of Things: From RFID to the Next-Generation Pervasive Networked Systems*, 1st ed. New York, NY, USA: Auerbach, 2008.
[11] P. V. Nikitin and K. V. S. Rao, "Performance limitations of passive UHF RFID systems," in *Proc. IEEE Antennas Propag. Soc. Int. Symp.*, Albuquerque, NM, USA, Jul. 2006, pp. 1011–1014.
[12] P. V. Nikitin, S. Ramamurthy, R. Martinez, and K. V. S. Rao, "Passive tag-to-tag communication," in *Proc. IEEE Int. Conf. RFID (RFID)*, Apr. 2012, pp. 177–184.
[13] G. Morocco and S. Caizzone, "Electromagnetic models for passive tag-to-tag communications," *IEEE Trans. Antennas Propag.*, vol. 60, no. 11, pp. 5381–5389, Nov. 2012.
[14] J. Ryoo, J. Jian, A. Athalye, S. R. Das, and M. Stanacevic, "Design and evaluation of 'BTTN': A backscattering tag-to-tag network," *IEEE Internet Things J.*, vol. 5, no. 4, pp. 2844–2855, Aug. 2018.
[15] Y. Karimi, A. Athalye, S. R. Das, P. M. Djuric, and M. Stanacevic, "Design of a backscatter-based tag-to-tag system," in *Proc. IEEE Int. Conf. RFID (RFID)*, May 2017, pp. 6–12.
[16] T. Lassouaoui, F. Hutu, Y. Duroc, and G. Villemaud, "Theoretical BER evaluation of passive RFID tag-to-tag communications," in *Proc. IEEE Radio Wireless Symp. (RWS)*, Jan. 2020, pp. 213–216.
[17] L. Zhou, F. Hutu, G. Villemaud, and Y. Duroc, "Simulation framework for performance evaluation of passive RFID tag-to-tag communications," in *Proc. 11th Eur. Conf. Antennas Propag. (EUCAP)*, Mar. 2017, pp. 500–504.
[18] H. Baker and A. LaGrone, "Digital computation of the mutual independance between thin dipoles," in *IRE Trans. Antennas Propag.*, vol. 10, no. 2, pp. 172–178, Mar. 1962, doi: 10.1109/TAP.1962.1137835.
[19] I. Adjali, A. Gueye, B. Poussot, S. Mostarshedi, F. Nadal, and J.-M. Laheurte, "Statistical study of coupling in randomly distributed dipole sets," in *Proc. 12th Eur. Conf. Antennas Propag. (EuCAP)*, 2018, pp. 1–5.
[20] T. Lassouaoui, F. Hutu, G. Villemaud, and Y. Duroc, "Modulation depth enhancement for randomly arranged tags in passive RFID tag to tag communications," in *Proc. IEEE Int. Conf. RFID Technol. Appl. (RFID-TA)*, Oct. 2021, pp. 116–119.
[21] Z. Liu, C. Zhang, Y. Li, Z. Wang, and Z. Wang, "A novel demodulator for low modulation index RF signal in passive UHF RFID tag," in *Proc. IEEE Int. Symp. Circuits Syst.*, May 2009, pp. 2109–2112, doi: 10.1109/ISCAS.2009.5118211.

TARIK LASSOUAOUI (Student Member, IEEE) was born in Casbah, Algeria. He received the M.Sc. degree in photonics and applied electronics from the University of Science and Technology of Algiers (USTHB), in 2016, and the M.Sc. degree in high frequency communications systems from the University of Marne-la-Vallée (UPEM), in 2018. He is currently pursuing the Ph.D. degree. His research interests include the electromagnetic theory, RFID design and measurements, scatter radio, and passive RFID tag to tag communications for the IoT.

FLORIN DORU HUTU (Senior Member, IEEE) was born in Iasi, Romania, in 1979. He received the Engineering degree in electronics and telecommunications and the master's degree in digital radio-communications from the Faculty of Electronics, Telecommunications and Information Technology, Gheorghe Asachi Technical University of Iasi, in 2003 and 2004, respectively, and the Ph.D. degree in automatic control from the University of Poitiers, France, in 2007. After two years of a postdoctoral position with the XLIM Laboratory, in September 2010, he became an Associate Professor with INSA Lyon, France. He joined the INSA Lyon's Electrical Engineering Department and the INRIA's Socrate Team of CITI Laboratory. He is the author of more than 80 national and international scientific articles. His research interests include energy efficient radio communications (wake-up radio, energy harvesting, and wireless power transfer) and RFID technologies. He is also involved in the design of software defined radio architectures for the IoT.

YVAN DUROC (Senior Member, IEEE) received the teaching degree Agregation (French national degree) in applied physics and the Ph.D. degree in electrical engineering from the Grenoble Institute of Technology, Grenoble, France, in 1995 and 2007, respectively. He was a Teaching Associate, from 1997 to 2009, and an Associate Professor, from 2009 to 2013, with the Esisar Engineering School Valence, France. He is currently a Full Professor with the University Claude Bernard Lyon 1, Villeurbanne, France. He is also an in-charge of lectures in signal processing, RF and microwave, electronics and embedded systems for the engineering and the M.Sc. levels. His current research interests include microwave and applied signal processing with special attention to radio frequency identification technologies, backscattered modulations, energy harvesting, time-reversal techniques, sensors, and antennas.

GUILLAUME VILLEMAUD (Senior Member, IEEE) received the M.S. degree in electrical engineering from the University of Limoges, France, in 1999, and the Ph.D. degree in electronics, in 2002.

From 1999 to 2002, he worked at IRCOM, Limoges, France, on compact integrated antennas. He developed multi-band hybrid arrays for mobile phone localization for CREAPE, from 2002 to 2003, and then joined the CITI Laboratory, Lyon, France, in 2003. He is currently an Associate Professor at INSA Lyon, the Head of the International Exchange Office with the Electrical Engineering Department and a member of the Executive Committee. He has published more than 100 international technical papers. His research interests include antenna design and integration, antenna diversity and multiple antenna processing (SIMO, MIMO), and system level simulation, coverage prediction, radio propagation, and measurements. He is currently the Site Leader for the FP7 Project iPlan for the development of planning and optimization tools for the deployment of Femtocells, also responsible of the Flexible radio terminals' axis of the INRIA SOCRATE Team. He is also strongly involved in the development of the Cognitive Radio platform, part of the Future Internet of Things equipment of excellence funded by the French government.